基于观测器与前馈的送丝机模糊 PI速度控制

杜宏旺[1,3], 刘 铮[2], 赵亚楠[1], 徐建伟[1], 刘 刚[1]

(1. 哈尔滨工程大学 机电工程学院, 哈尔滨 150001;
2. 哈尔滨工程大学 计算机科学与技术学院, 哈尔滨 150001;
3. 哈尔滨工程大学 自动化学院, 哈尔滨 150001)

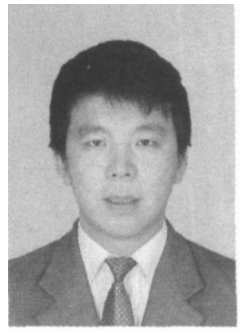

杜宏旺

摘 要: 送丝系统是焊接机器人的重要组成部分, 稳定可靠的送丝是保证焊接质量的前提; 焊丝从丝盘上抽取和经过绝缘管与导电嘴的过程中受到的阻力呈严重的非线性, 所受的阻力严重影响送丝速度和焊接质量. 采用状态观测对阻力进行观测, 并根据观测值对系统进行前馈, 以提高系统的速度响应, 消除送丝阻力对系统的影响. 因为电机存在阻尼, 采用常规 PI控制可以改善系统的稳态特性, 抑制稳态误差; 把模糊控制和 PI控制有机地结合起来, 利用模糊控制的动态响应和 PI控制的稳态性能, 实现送丝机安全可靠的送丝; 仿真表明采用状态观测和前馈控制速度响应快、超调小、鲁棒性强, 模糊 PI控制较传统 PI控制有更好的动、静特性; 接管焊接试验结果表明焊接质量完全达到规定要求.

关键词: 送丝机; 埋弧焊; 状态观测器; 前馈; 模糊 PI
中图分类号: TP273 文献标识码: A 文章编号: 0253-360X(2010)01-0085-04

0 序 言

在机器人自动焊接设备中, 送丝机多采用直流电机[1], 因其具有运动效率高、启动力矩大、启动电流小、噪音低、使用寿命长和便于调速的优点; 目前, 自动焊接基本上采用送丝机对焊丝进行进给, 多采用 PID控制器对送丝机进行控制; 因为焊接过程中焊丝带电, 必须对焊丝与机器人接触的地方进行绝缘, 采用绝缘管或者绝缘支架进行绝缘; 当焊丝从焊盘上抽取的时候会产生阻力, 无论是拉丝还是推丝方式, 当焊丝经过送丝软管或者绝缘支架时产生进给阻力和摩擦力, 而且焊丝从丝盘到焊点之间的距离越长, 送丝阻力越大; 这些阻力和摩擦力都呈现出严重的非线性, 难以进行测量. 在机器人焊接过程中, 当各手臂运动时, 焊丝会随着送丝软管的弯曲或绝缘支架的运动而产生弯曲, 致使送丝阻力时刻在变化, 会对送丝机的送丝速度产生扰动, 尤其当送丝速度按照焊接要求进行变化时, 严重影响焊接质量.

一般情况下, 这种负载干扰具有不确定性且非线性很强, 使干扰的测量变得困难, 为了解决此问题, 文中采用状态观测器对送丝机的负载干扰进行观测, 这样就根据负载干扰量的观测值对系统干扰实时地进行前馈补偿, 消除扰动对系统的影响; 通过这种方法可以减小负载干扰引起的速度误差和位置误差, 提高送丝机对负载的抗干扰能力. 直流电机本身是一个非线性的被控对象; 许多拖动负载含有弹性或间隙等非线性因素, 使得常规 PI控制器参数难以达到最优状态, 而参数的一成不变难以跟随现场的动态变化, 针对上述问题, 提出一种基于 FUZZY-PI控制的直流调速系统来克服常规 PI控制的不足, 并提高系统的动态响应和稳态特性.

收稿日期: 2009-06-02

1 直流电机的数学模型

根据电机电枢回路电压方程、反电动势、力矩方程和力平衡方程可得直流电机数学模型[2]

$$\left.\begin{aligned} L_a\frac{di_a}{dt}+R_a i_a+e&=U_a\\ e&=C_e\theta_m\\ T_m&=C_m i_a\\ T_m&=T_L+J_m\ddot{\theta}_m \end{aligned}\right\} \quad (1)$$

式中: R_a和 L_a分别为电枢电阻和电感; C_m为电动机的转矩常数; T_L为负载转矩; J_m为折算到电机输出轴上的转动惯量; C_e为电势常数; θ_m为系统速度; $\ddot{\theta}_m$为系统加速度.

2 负载状态观测器及前馈

采用状态观测对电机力矩平衡方程中的负载转矩和摩擦转矩进行观测[3-6]，其中负载转矩包括摩擦力矩和焊丝进给过程产生的扰动力矩等；另外，跟据状态观测器观测到的观测值对系统进行前馈，以消除负载转矩对系统影响.

2.1 状态观测器的设计

根据牛顿力学定律得到电机的力矩平衡方程为

$$T_m = T_L + J_m\dot{\theta}_m + B_m\theta_m \tag{2}$$

式中：B_m为粘滞摩擦系数.

带负载观测器直流电机系统框图如 1所示.

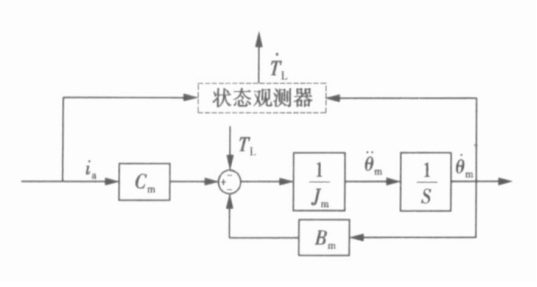

图 1 带负载观测器直流电机力矩平衡系统框图

Fig. 1 Block diagram of DC motor torque-balance equation with load observer

由式(2)可得

$$\begin{bmatrix}\dot{T}_L\\ \dot{\theta}_m\end{bmatrix} = \begin{bmatrix}0 & 0\\ -\frac{1}{J_m} & -\frac{B_m}{J_m}\end{bmatrix}\begin{bmatrix}T_L\\ \theta_m\end{bmatrix} + \begin{bmatrix}0\\ \frac{C_m}{J_m}\end{bmatrix} i_a$$

$$y = [0 \quad 1]\begin{bmatrix}T_L\\ \theta_m\end{bmatrix} \tag{3}$$

式中：θ_m是系统的速度输出，是可测的物理量；T_L是待测物理量，现进行可观测性分析为

$$\mathrm{rank}\begin{bmatrix}C\\ CA\end{bmatrix} = \mathrm{rank}\begin{bmatrix}0 & 1\\ -\frac{1}{J_m} & -\frac{B_m}{J_m}\end{bmatrix} = 2 \tag{4}$$

故系统的观测性矩阵的秩为 2，符合满秩的要求，故该系统是可观测的；对于上式显然有 $A_{11}=0$，$A_{12}=0$，$A_{21}=-\frac{1}{J_m}$，$A_{22}=-\frac{B_m}{J_m}$，$B_1=0$，$B_2=\frac{C_m}{J_m}$，$C_1=0$，$C_2=1$. 为使 $\dot{T}_L \to T_L$，需要使 $A_{11}-G_1A_{21}<0$ 在一维情况下使 $G_1=g_1$，并取 $g_1=-S_* \cdot J$ ($-S_*<0$)，则有

$$\begin{aligned}\dot{z} &= (A_{11}-G_1A_{21})z + (B_1-G_1B_2)u + [(A_{11}-G_1A_{21})G_1 + (A_{12}-G_1A_{22})]y\\ &= \frac{g_1}{J_m}z - \frac{C_m g_1}{J_m} i_a + \left(\frac{g_1^2}{J_m} + \frac{B_m g_1}{J_m}\right)\theta_m\end{aligned} \tag{5}$$

由于

$$\left.\begin{aligned}\hat{x}(s) &= z(s) + g_1 y(s)\\ \hat{y}(s) &= \hat{x}(s)\end{aligned}\right\}$$

对上式进行拉普拉斯变换并化简可得到

$$\hat{T}_L = \hat{x}(s) = \frac{-C_m g_1 i_a(s) + (g_1^2 + B_m g_1 + G_1 J_m s - g_1)\theta_m(s)}{J_m s - 1} \tag{6}$$

$\hat{T}_L$即为通过对力矩方程输入量 $i_a(s)$和输出量 $\theta_m(s)$进行观测得到观测值的拉普拉斯函数.

2.2 前馈传递函数的求解

对直流电机的数学模型进行整理，并加上负载状态观测器和前馈，进行整理获得如图 2所示的基于负载观测器与前馈的直流电机系统框图.

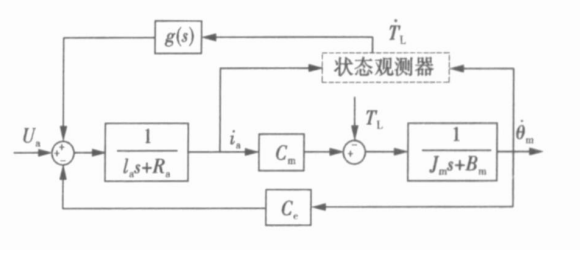

图 2 基于观测器与前馈的直流电机系统框图

Fig. 2 Block diagram of DC motor based on state observer and feedforward

由图 2可得

$$\theta_m = (\hat{T}_L \cdot g(s) + U_a)\frac{C_m}{(l_a s + R_a)\cdot(J_m s + B_m) + C_m \cdot C_e} - T_L \cdot \frac{l_a s + R_a}{(l_a s + R_a)\cdot(J_m s + B_m) + C_m \cdot C_e} \tag{7}$$

理论上 $\hat{T}_L \to T_L$，即认为观测值趋近于实际值 $\hat{T}_L \to T_L$，若取：$\hat{T}_L \cdot g(s) \cdot C_m - T_L \cdot (l_a s + R_a) = 0$ 则可以看出观测值 $\hat{T}_L$完全补偿扰动信号 T_L对系统输出的影响，这样，前馈通道的传递函数 $g(s)$可以由式(7)确定，即可以获得前馈传递函数为

$$g(s) = \frac{l_a s + R_a}{C_m} \tag{8}$$

3 FUZZY—PI控制器的设计

采用状态观测器和前馈可以极大地增强系统的抗干扰能力，比例+积分(PI)控制器可以使系统在进入稳态后无稳态误差；但传统的 PI不能根据负载变化和系统特性变化调节控制器参数，因此提出采

用模糊 PI[7,8]来满足系统的要求，模糊 PI是在 PI算法的基础上，通过计算当前的系统误差和误差变化率，利用模糊规则进行模糊推理，查询 PI规则表进行模糊推理，查询模糊规则对 PI参数进行在线调整，其原理图如图 3所示.

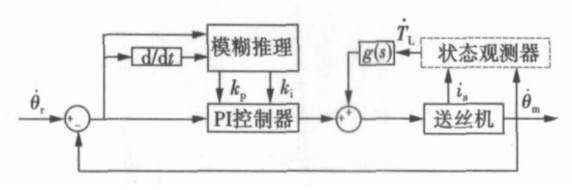

图 3　基于观测器与前馈直流电机的模糊 PI控制

Fig. 3　Fuzzy-PI control in DC motor based on state observer and feedforward

模糊 PI参数的在线调整克服了参数在调整的整个过程固定不变的特点，适应性更强，其算法为：$\Delta k_p = f_1(e, ec)$；$\Delta k_i = f_2(e, ec)$；$k_p = k_{p0} + \Delta k_p$；$k_i = k_{i0} + \Delta k_i$，其中：$\Delta k_p$和 Δk_i分别为偏差 e和偏差变化率 ec对应于模糊规则表中的输出值；k_{p0}和 k_{i0}分别为比例系数和积分系数的初始值.

3.1　模糊规则

从系统的稳定性、超调量和稳态精度等方面考虑，综合 Δk_i和 Δk_p对系统的不同作用以及二者之间的相互作用关系建立的模糊规则见表 1，表 2.

表 1　Δk_i的模糊规则表

Table 1　Fuzzy rule table of Δk_i

Δk_i e \ ec	NB	NM	NS	ZO	PS	PM	PN
NB	NB	NB	NM	NM	NS	ZO	ZO
NM	NB	NB	NM	NS	NS	ZO	ZO
NS	NB	NM	NS	NS	ZO	PS	PS
ZO	NM	NM	PS	ZO	PS	PM	PM
PS	NM	NS	ZO	PS	PS	PM	PB
PM	ZO	ZO	PS	PS	PM	PB	NB
PN	ZO	ZO	PS	PM	PM	PB	PB

3.2　隶属度函数

系统的误差 e和误差变化率 ec变化范围定义为模糊集上的论域，$e, ec = [-5\ 5]$，其模糊子集，$e, ec = \{NB, NM, NS, Z, PS, PM, PB\}$；$\Delta k_i$和 Δk_p的论域分别为 $[-2\ 2]$，$[-4.5\ 4.5]$，两者的模糊子集均为 $\{NB, NM, NS, Z, PS, PM, PB\}$. e与 ec，Δk_i，Δk_p的隶属度函数如图 4所示.

3.3　仿真

与直流电机直接相连的减速器的减速比 $i=40$，送丝轮半径为 20 mm，送丝速度为 3 mm/s，则送丝轮旋转速度为 24 转/min，并根据实际模型在 Matlab[9]进行仿真.

表 2　Δk_p的模糊规则表

Table 2　Fuzzy rule table of Δk_p

Δk_p e \ ec	NB	NM	NS	ZO	PS	PM	PN
NB	PB	PB	PM	PM	PS	ZO	ZO
NM	PB	PB	PM	PS	PS	ZO	NS
NS	PM	PM	PM	PS	ZO	NS	NS
ZO	PM	PM	PS	ZO	NS	NM	NM
PS	PS	PS	ZO	NS	NS	NM	NM
PM	PS	ZO	NS	NM	NM	NM	NB
PN	ZO	ZO	NM	NM	NM	NB	NB

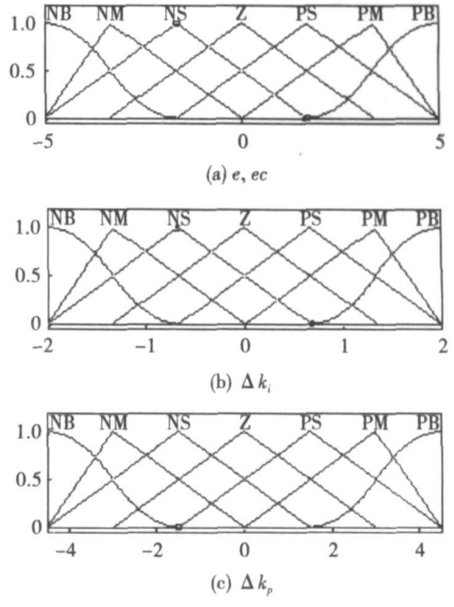

图 4　隶属度函数

Fig. 4　Affiliation function

3.4　模糊 PI与传统 PI的对比

当状态观测器和前馈不参与到当中时，比较图 5和图 6可以看出，当采用模糊 PI控制时，能明显改善系统的动态特性，减小系统超调量和系统的

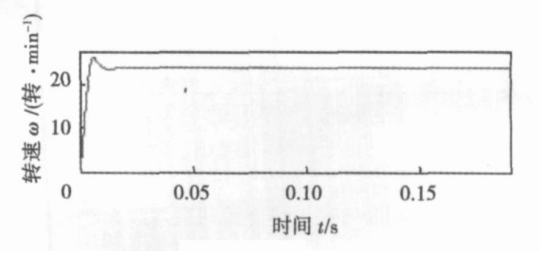

图 5　当观测器与前馈不参与控制时的 PI控制

Fig. 5　Speed response without state observer and feedforward participating in PI control

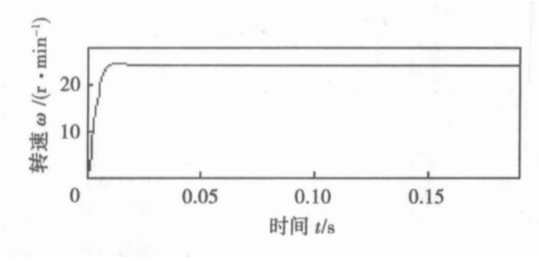

图 6 当观测器与前馈参与控制时的模糊 PI控制

Fig. 6 Speed response without state observer and feedforward participating in Fuzzy PI control

调节时间.

3.5 模糊 PI控制下状态观测器和前馈参与控制

在模糊 PI控制条件下当状态观测器和前馈不参与到控制当中时，突然施加载荷，系统的速度响应见图 7；在模糊 PI控制条件下当状态观测器和前馈参与到控制当中时，突然施加载荷，系统的速度响应见图 8. 经过对比可发现，当状态观测器和前馈控制参与到控制中时，超调量和调节时间明显小很多，送丝机的速度输出几乎没受到影响. 可以看出，负载观测器的观测值引入到控制环的输入端，提高了系统的抗扰动态性能，补偿了系统阻尼和因为扰动而存在的速度差，从而使系统对扰动的鲁棒性得到了明显提高，同时也提高了伺服系统的稳态精度，极大地减小了送丝机因送丝阻力而产生的速度扰动.

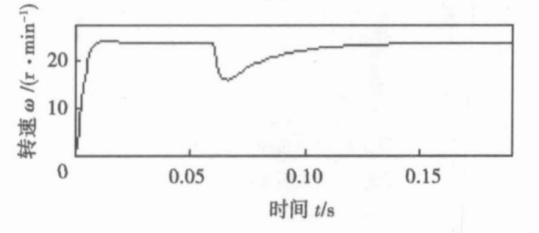

图 7 当状态观测器与前馈不参与控制突加载荷时的模糊 PI 控制的速度响应

Fig. 7 Speed response without state observer and feedforward participating in Fuzzy PI control when DC motor was loaded adruptly

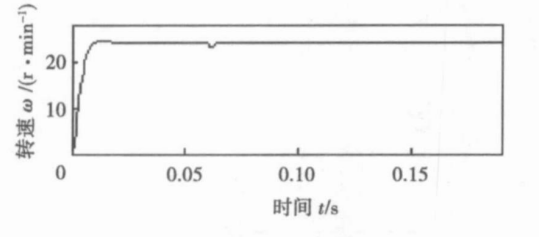

图 8 当状态观测器与前馈参与控制突加载荷时的模糊 PI 控制的速度响应

Fig. 8 Speed response with state observer and feedforward participating in Fuzzy PI control when DC motor was loaded adruptly

4 试 验

试验为压力容器正马鞍形接管的焊接，焊接方式埋弧焊，接管直径为 200 mm，筒体直径为 6 000 mm，接管轴心与筒体轴心垂直相交，即为正马鞍接管焊接；焊接电流 600 A，电压 40 V，焊丝直径为 2 mm. 图 9a为接管焊接填充完毕后的焊接表面；当接管焊接完成一圈后为实现连续焊接进行的焊接变轨处如图 9b所示. 在焊接过程中，形成连续的焊缝，焊接过程稳定；在变轨处，机器人手臂快速运动，焊丝在丝盘和焊点之间的路径发生变化，导致送丝阻力发生变化，从而对送丝速度产生不良影响，采用观测器观测阻力后进行前馈有效地抑制了送丝速度的变化. 可以看出在变轨处焊接连接良好，整个焊接过程中没有发生咬边、夹渣、焊瘤、焊坑、焊道宽窄不齐和焊缝外形尺寸过大的现象；X射线探伤检查，合格率为 100%，完全达到焊接质量要求. 囿于篇幅，文中不就焊接填充策略、变轨方式、送丝速度与机器人末端关节运动速度协调进行讨论.

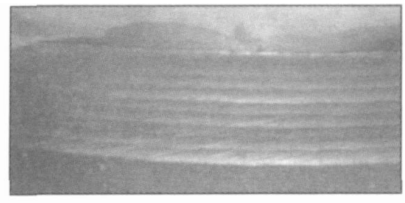

(a) 连续焊接处的焊道

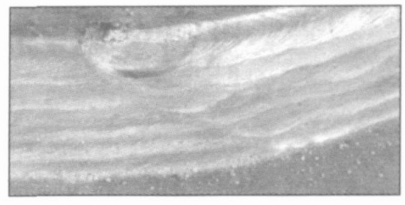

(b) 连续焊接变轨处的焊道

图 9 焊接试验

Fig. 9 Welding experiments

5 结 论

(1) 采用状态观测器对送丝阻力扰动进行观测，并根据直流电机模型求解前馈传递函数进行前馈，此方法改善了系统动态性能，增强了系统抗干扰能力，极大地降低了送丝阻力扰动对电机输出速度

[下转第 92 页]

TIG焊接工艺进行 5A06-O铝合金焊接，复合高频脉冲电流频率大小对 5A06-O铝合金焊接接头的组织和力学性能产生了重要影响，适当选择复合脉冲方波电流频率，可达到细化焊缝组织，降低焊接接头软化程度的目的，有利于改善和提高 5A06-O铝合金的焊接质量.

(2)保持脉冲电流幅值 70 A，占空比 50%不变，在脉冲电流频率为 40 kHz的条件下，5A06-O铝合金焊接接头抗拉强度和断后伸长率分别可达到母材金属的 95.8%和 84.8%.

参考文献：

[1] 姚君山，徐 萌，柴 鹏 等. 推进剂贮箱先进焊接工艺研究进展[J]. 航空制造技术，2008，8：32－35.
Yao Junshan, Xu Meng, Chai Peng et al. Research progress of advanced welding technique for propellant tank[J]. Aeronautical Manufacturing Technology, 2008, 8: 32－35.

[2] 李晓红，毛 唯，熊华平. 先进航空材料和复杂构件的焊接技术[J]. 航空材料学报，2006，26(3)：276－282.
Li Xiaohong, Mao Wei, Xiong Huaping. Welding technologies of advanced aeronautical materials and complex-shaped structural components[J]. Journal of Aeronautical Materials, 2006, 26(3): 276－282.

[3] 廖希亮. 脉冲电流对金属凝固组织的影响[D]. 上海：上海大学，2007.

[4] 班春燕. 电磁场作用下铝合金凝固理论基础研究[D]. 沈阳：东北大学，2002.

[5] 齐铂金，从保强. 超快变换方波复合脉冲电流变极性弧焊电源装置：中国，200710120834.6[P]. 2008－02－20.

[6] 齐铂金，从保强. 新型超快变换复合脉冲变极性弧焊电源拓扑[J]. 焊接学报，2008，29(11)：57－60.
Qi Bojin, Cong Baoqiang. A novel ultrafast-convert complex pulse variable polarity arc welding power topology[J]. Transactions of the China Welding Institution, 2008, 29(11): 57－60.

[7] 姚君山，周万盛. 铝及铝合金的焊接[M]. 北京：机械工业出版社，2006.

[8] 屠海令，干 勇. 金属材料理化测试全书[M]. 北京：化学工业出版社，2006.

[9] 刘正义，吴连生，许麟康，等. 机械装备失效分析图谱[M]. 广州：广东科技出版社，1990.

作者简介：从保强，男，1979年出生，工学博士. 主要研究方向为焊接过程控制、新型弧焊电源技术及应用等方面. 发表论文 8篇.
Email: congbq@163.com

[上接第 88页]
的影响.

(2)模糊 PI较传统 PI具有能明显改善系统的动态性能和稳态特性，减小系统超调量和系统的调节时间，使用这种方法可提高送丝速度的控制精度.

(3)结果表明，采用状态观测器对阻力扰动进行观测并对阻力观测值进行前馈扰动补偿，并采用模糊 PI方法对送丝机进行控制，是一种送丝机实现连续变速焊接并能保证焊接质量的可靠方法.

参考文献：

[1] 李 焰. MIG/MAG焊送丝机控制系统[J]. 焊接学报，1991，12(1)：59－63.
Li Yan. Wire feeder control system for MIG/MAG welding[J]. Transactions of the China Welding Institution, 1991, 12(1): 59－63.

[2] 王 岚. 基于 Fuzzy控制的零重力操作系统[J]. 模式识别与仿真技术，2005，12(24)：48－50.
Wang Lan. Zero gravity operation system based on fuzzy control[J]. Pattern Recognition and Simulation, 2005, 12(24): 48－50.

[3] Chen Rong. Rearch on resist-disturbance performance of servo system based on load observer[J]. Proceedings of the CSEE, 2008, 24(8): 103－108.

[4] Wey T. Modeling and observer design for hydraulic cylinders[C] // IEEE Mediterranean Conference on Control and Systems, Italy. IEEE, 1995: 1－6.

[5] Kim C S, Lee C O. Speed control of an overcentered variable-displacement hydraulic motor with a load-torque observer[C] // Control Engineering Practice, Britain. IEEE, 1993: 1563－1570.

[6] Ugur Tumerdem. Haptic consensus in Bilateral teleoperation[C] // Proceedings of Internatconel Conference on Mechatronics, Japan. IEEE, 2007: 1－6.

[7] Tunyasrirut S. Adaptive fuzzy PI controller for speed of separately excited DC motor[C] // Proceedings of the IEEE International Conference on Systems, China, Man and Cybernetics, 1999: 196－201.

[8] 刘金琨. 先进 PID控制及其 MATLAB仿真[M]. 北京：电子工业出版社，2003.

[9] 亨塞尔曼. 精通 Matlab 7[M]. 北京：清华大学出版社，2006.

作者简介：杜宏旺，男，1975年出生，博士研究生. 主要从事机器人的研究. 发表论文 7篇.
Email: duhongwang@yahoo.com.cn

plasma arc are also investigated. The results show that it is feasible to control the shape and heat flow density of the plasma arc for the transverse alternating magnetic field, which can expand the area of plasma arc thermal treatment and flat the heat flow density upon the workpiece. Furthermore, the oscillating amplitude of plasma arc increases and the heat flow density gradient upon the workpiece decreases with the magnetic flow density enhancing. However, an overly strong magnetic field coil results in the plasma arc unstable. Under the same magnetic flow density, less gas flow rate and arc current, longer distance from the nozzle outlet to the anode causes the oscillating amplitude to increase. Contrarily, the more gas flow rate and arc current, the more heat flow density peak increases. Moreover, longer distance from nozzle outlet to workpiece descends the heat flow density peak.

Key words: transverse alternating magnetic field (TAMF); plasma arc; oscillating amplitude; heat flow density distribution

Experimental investigation on impact toughness in high-temperature of BHW35 steel welded joint WANG Xiangyun[1,2], WANG Wenxian[1], LI Jiemu[3], WANG Baodong[3] (1. College of Materials Science and Engineering, Taiyuan University of Technology, Taiyuan 030024, China; 2. Taiyuan Boiler Group Co. Ltd., Taiyuan 030021, China; 3. Shanxi Zhongtong High-Technology Co., Taigu 030008, Shanxi, China). p80—84

Abstract: Automatic submerged-arc welding and shielded metal arc welding were employed by H10Mn2NiMoA welding wires, E7015-D2 electrode followed by the postweld heat treatment systems of normalizing, drawing temper and stress relief annealing. Impact tests on welded joint and base metal at 20 ℃, 100 ℃, 200 ℃ and 350 ℃ were carried out. Furthermore, SEM fractograph, metallograph and chemical compositions of welding seam were analyzed. The results indicate that the highest hardness of HAZ was 270.5 HV in SAW, 235.2 HV in SMAW, the toughness increases greatly compared with conditions at room temperature. Peak value of impact toughness of SAW is at 100 ℃, SMAW is at 200 ℃, which is close to that of base metal. The impact toughness in HAZ is better than that in welding seam, and it is better in SMAW than that in SAW. The impact toughness of welded joint is upward 96.33 J at room temperature, it is upward 120 J in welded joint at 350 ℃, and 186 J in base metal, which indicate that the toughness of welded joint and base metal ars in their best at room and high-temperature. SEM fractograph indicates that all impact fractures exhibit ductile dimple, the better toughness, the more obvious tearing feature of ductile dimple. The larger the ductile dimple is, the more obvious nonuniform distribution is.

Key words: BHW35 steel; welded joint; metallograph and hardness; impact toughness; fractograph

Fuzzy PI speed control for welding wire feed system based on state observer and feedforward DU Hongwang[1,3], LIU Zheng[3], ZHAO Yanan[3], XU Jianwei[3], LIU Gang[2] (1. College of Mechanical and Electrical Engineering, Harbin Engineering University, Harbin 150001, China; 2. College of Computer Science and Technology, Harbin Engineering University, Harbin 150001, China; 3. College of Automation, Harbin Engineering University, Harbin 150001, China). p85—88

Abstract: Welding wire feeding device is an important component of welding robot, stabilization and reliability of welding wire feed is the essential for welding quality. The resistance was highly nonlinear and both wire feed rate and welding quality are severely affected by the resistance. A state observer was adopted to evaluate the resistance, and then the observed resistance was forward fed in order to increase speed response and eliminate the impact of resistance on the welding wire feed system. Because of DC motor damping, the steady-state characteristics can be improved and the steady-state error can be inhibited when conventional PI control is adopted. The fuzzy control and PI control are organically introduced by means of dynamic response of fuzzy control and steady-state performance of PI control, it is reliable to achieve stable welding wire feeding. The simulations indicate that there are fast speed response, small overshoot and strong robustness with state observer and forward feed, the dynamic and static characteristics of fuzzy PI control are better than PI control.

Key words: wire feed device; submerged-arc welding; state observer; feedforward; fuzzy PI control

Effect of hybrid-pulse square-wave current frequency on microstructure and mechanical properties of 5A06 aluminum alloy welds CONG Baoqiang, QI Bojin, ZHOU Xingguo, LUO Jun (School of Mechanical Engineering and Automation, Beihang University, Beijing 100191, China). p89—92

Abstract: A novel ultrafast-convert hybrid-pulse square-wave variable polarity arc welding technology for aluminum alloy is developped. Based on the hybrid-pulse variable polarity TIG welding technique, the effect of hybrid-pulse square-wave current frequency on the microstructure and mechanical properties of 5A06 welds is researched. The experimental results show that, compared with no hybrid-pulse current, the weld mechanical properties are decreased when the pulse current frequency is less than 20 kHz. Under the condition of pulse current frequency up to 40 kHz, the size of crystal grains and degree of welds softening are decreased, tensile strength of weld joints is improved obviously. The rates of weld tensile strength and percentage elongation to base metal are 95.8% and 84.8%, respectively.

Key words: ultrafast-convert; hybrid high-frequency pulse; pulse frequency; variable polarity; aluminum alloy

Wavelet detection algorithm of short-circuit signal in CO_2 arc welding based on DSP TIAN Songya, GU Haitao, FU Weiliang, SHI Rusen, XU Huizhe (College of Mechanical & Electrical Engineering, Hohai University, Changzhou 213022, Jiangsu, China). p93—96

Abstract: According to algorithm arrous and analysis of CO_2 arc voltage characteristic by Wavelet Toolbox in Matlab, the wavelet algorithm which is suitable for detection of short-circuit signal in practical CO_2 welding process is derived. Different